

OVA-Det: Open Vocabulary Aerial Object Detection with Image-Text Collaboration

Guoting Wei^{1,4}*, Xia Yuan¹*, Yu Liu³*, Zhenhao Shang², Xizhe Xue², Peng Wang², Kelu Yao³,
Chunxia Zhao¹, Haokui Zhang^{2,4}†, Rong Xiao⁴

¹Nanjing University of Science and Technology ³Zhejiang Lab

²Northwestern Polytechnical University ⁴IntelliFusion Inc.

Abstract

Aerial object detection plays a crucial role in numerous applications. However, most existing methods focus on detecting predefined object categories, limiting their applicability in real-world open scenarios. In this paper, we extend aerial object detection to open scenarios through image-text collaboration and propose OVA-Det, a highly efficient open-vocabulary detector for aerial scenes. Specifically, we first introduce an image-to-text alignment loss to replace the conventional category regression loss, thereby eliminating category limitations. Next, we propose a lightweight text-guided strategy that enhances the feature extraction process in the encoder and enables queries to focus on class-relevant image features within the decoder, further improving detection accuracy without introducing significant additional costs. Extensive comparison experiments demonstrate that the proposed OVA-Det outperforms state-of-the-art methods on all three widely used benchmark datasets by a large margin. For instance, for zero-shot detection on DIOR, OVA-Det achieves 37.2 mAP and 79.8 Recall, 12.4 and 42.0 higher than that of YOLO-World. In addition, the inference speed of OVA-Det reaches 36 FPS on RTX 4090, meeting the real-time detection requirements for various applications. The code is available at <https://github.com/GT-Wei/OVA-Det>.

1. Introduction

Aerial object detection, which involves localizing and categorizing objects of interest within aerial images, has become increasingly important due to its broad application requirements, including earth monitoring, disaster search, and rescue [7, 21, 30]. Most existing aerial detectors [15, 19, 25, 38] can only identify predefined categories from

*Equal contribution.

†Corresponding author.

This work was done during Guoting Wei's internship at IntelliFusion.

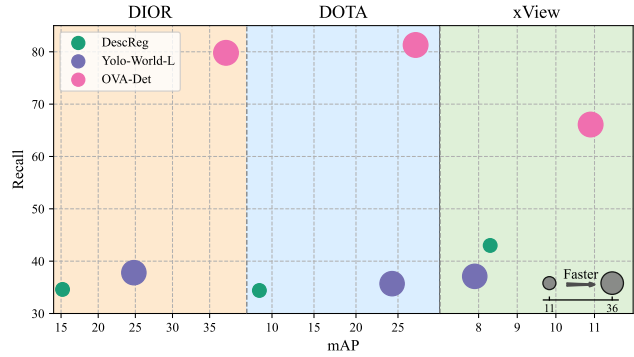


Figure 1. Comparison of OVA-Det with other advanced open-vocabulary detectors on the DIOR, DOTA, and xView datasets in terms of Recall, mAP, and FPS. Marker size encodes FPS, such that bigger markers indicate faster inference. All models are evaluated in a zero-shot detection setting.

their training sets, which strictly restrict their deployment in open-world scenarios, which have become key considerations for real-world applications. A major obstacle for these detectors in discovering novel classes is their reliance on mapping image features to a fixed set of class indices [12].

Recently, CLIP [28] has the capability to map vision-language features into a comparable representation space. This offers an opportunity to break the category limitations inherent in traditional object detection. Inspired by this, several works [4, 11, 24, 45] on natural images have explored the relationship between images and text to endow models with open-vocabulary detection capabilities, achieving notable success. For instance, VILD [11] and VL-PLM [45] use pre-trained VLM to classify the object proposals generated by region proposal network. GLIP [22] formulates object detection as a phrase grounding task, thereby unifying these two tasks. The introduction of textual information and the synergy between image and text have significantly expanded the coverage of traditional object detection tasks, taking them a step closer to real-world applications in

open environments.

However, in the field of aerial object detection, such work remains very limited. Aerial object detection poses unique challenges, including predominantly small objects, varying viewpoints, and limited detection data. Directly applying existing open-vocabulary detection methods designed for conventional perspectives to aerial perspectives may result in suboptimal performance. Very recently, some researchers have attempted to address this gap and proposed insightful methods [23, 26, 40]. The introduction of these works has validated the potential of the open-vocabulary approach in the aerial object detection field, but there is still significant room for optimization. For instance, DescReg [40] introduces a description regularization method that focuses on enhancing textual descriptions but overlooks the importance of visual-semantic interaction. CastDet [23] adopts a complex multi-teacher framework based on a two-stage detector for open-vocabulary detection, which neglects the efficiency.

In this paper, we propose an efficient open-vocabulary detection model specifically designed for aerial photography scenes, termed OVA-Det. Specifically, we adopt the basic architecture of RT-DETR, due to RT-DETR has high inference efficiency and concise structure. First, we adapt the pretrained CLIP model and integrate it into the base framework to leverage its image-text alignment capability and powerful feature extraction, alleviating the limited sample problem. We then propose an image-to-text alignment loss to bridge the domain gap between natural images and aerial images, extending the model’s applicability from closed-world to open-world scenarios. Next, considering the challenges posed by long perception distances in aerial images, such as small detection targets with less prominent visual features and strong background interference, we propose to enhance visual feature and object queries in encoder and decoder with lightweight text guidance architectures, which further improving the detection accuracy without substantially increasing computational costs. Finally, extensive experiments are conducted to validate our method on three widely used benchmark datasets for zero-shot aerial object detection, as well as on two commonly adopted datasets for traditional closed-set aerial object detection. As illustrated in Figure 1, our proposed OVA-Det outperforms YOLO-World and DescReg in terms of mAP, Recall, and inference speed, demonstrating the effectiveness of our design.

In summary, there are three major contributions:

- We propose an image-to-text alignment loss as a bridge to address the modality gap between natural images and aerial images. By integrating it with CLIP, we extend the RT-DETR framework from closed-world to open-world scenarios.
- We introduce lightweight text-guidance architectures, text-guided feature enhancement (TG-FE) and text-

guided query enhancement (TG-QE) to enhance object visual features while suppressing background interference, further improving detection accuracy.

- Our method demonstrates SOTA on multiple widely used benchmark datasets for zero-shot detection, as well as in traditional aerial object detection tasks, while maintaining a high inference speed. For instance, the proposed OVA-Det achieves 37.2 mAP and 79.8 Recall, while maintaining 36 FPS. To the best of our knowledge, we are the first real time open-vocabulary aerial detection method.

2. Related Work

2.1. Open Vocabulary Object Detection

Traditional object detectors [1, 2, 29, 46] predominantly rely on fully supervised training, mapping image features to class indices [12]. Such detectors are limited to recognizing only the categories seen during training, known as fixed-vocabulary (closed-set) detection. In contrast, open-vocabulary object detection (OVD) aims to explore the relationship between image and text to enable detectors to identify classes beyond those in the training sets.

Inspired by CLIP [17, 28] establish image-text feature alignment, recent works have incorporated class semantic information into detectors, exploring open-vocabulary object detection. These approaches can be roughly divided into two types. The first type [3, 11, 20, 34, 45, 47] uses networks like FPN to extract object proposals, which are then classified using pre-trained VLMs. For example, VILD [11] enhances OVD capability by distilling knowledge from pre-trained VLMs. Similarly, VL-PLM [45] leverages pre-trained VLMs to generate region-text pair labels for unlabeled images, these labels are subsequently used to train the detector, enabling recognition of novel object categories not present in the original training set. The second type integrates detection and grounding tasks [4, 22, 24, 39, 44], aiming to collect sufficient data to train specialized VLMs from scratch for detection. For instance, GLIP [22] unifies object detection and phrase grounding tasks to pre-train a detector for open-vocabulary detection. Grounding DINO [24] incorporates the pre-training strategy into transformer detection [43] based on phrase grounding.

The most relevant work is YOLO-World [4], which extends YOLO to the open-vocabulary detection field through visual-language modeling. Firstly, YOLO-World and OVA-Det are proposed for different domains, natural images and aerial images. Secondly, the module design and loss function are also different. Unlike YOLO-World, which primarily uses text as guidance and focuses only on the feature extraction part, our proposed OVA-Det leverages text information to guide and enhance features in both the encoder and decoder with a concise architecture. This design is

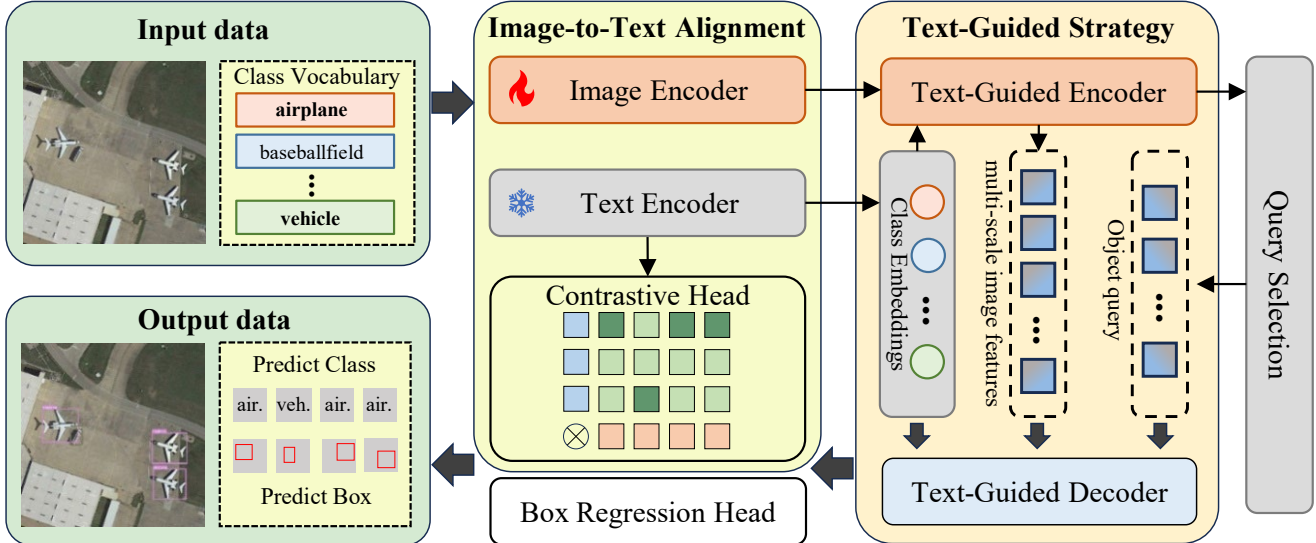


Figure 2. Overall architecture of OVA-Det. The proposed OVA-Det can be summarized into two main components: the Image-to-Text Alignment and the Text-Guided Strategy. (1) Image-to-Text Alignment connects visual objects with class embeddings rather than relying on class indices, which enables the model to detect classes beyond a predefined set. It involves a text encoder, a contrastive head, and a image-text alignment loss. (2) Text-Guided Strategy explores cross-modal interaction to enhance class-relevant feature extraction and suppress background interference, forming a text-guided encoder-decoder structure.

more effective in addressing the unique challenges of aerial images, such as low-quality and various viewpoints issues. Furthermore, the image-to-text alignment loss in OVA-Det replaces bidirectional alignment with unidirectional alignment, reducing optimization difficulty. These differences allow OVA-Det to achieve better performance in the aerial domain.

2.2. Aerial Object Detection

Previous studies [8, 15, 19, 38] on aerial object detection have predominantly employed deep neural networks and coarse-to-fine architectures to enhance detection performance. However, these methods, functioning as closed-set detectors, are inherently limited in their ability to recognize unseen categories. Only a few works [23, 26, 40] explore open-vocabulary detection for aerial images. DescReg [40] argues that aerial images exhibit a weak semantic-visual correlation and utilizes a triplet loss to preserve the visual similarity structure within the classification space, thereby enhancing knowledge transfer from base to novel classes. CastDet [23] employs a semi-supervised training paradigm within a complex multi-teacher framework. It leverages a pre-trained vision-language model as a teacher to generate high-quality pseudo-labels for unlabeled images containing novel classes, thereby enabling the detection of object categories beyond those present in the training dataset. LAE-DINO [26] introduces a DINO-based detector that leverages dynamic vocabulary construction and visual-guided text prompt learning to explore class semantics, thereby en-

hancing OVD performance. These methods demonstrate the potential of the open-vocabulary approach in aerial object detection.

However, existing methods rely on complex architectures that overlook the efficiency demands in aerial detection and fail to fully exploit the benefits of image-text collaboration. In response, OVA-Det builds upon a lighter framework and adopts a text-guided strategy to propagate class embeddings as clues throughout the entire network, helping the model focus on class-relevant object features and suppress extensive background interference.

3. Method

3.1. Model Architecture

The overall architecture of OVA-Det is illustrated in Fig. 2. From the figure, we can see that the designs in the proposed OVA-Det focus on two major components: the image-to-text alignment component and the text-guided strategy component. The former is proposed to overcome category limitations. We integrate class embeddings via a text encoder, constructing both a contrastive head and an image-to-text alignment loss to facilitate image-text alignment. The latter is designed to enhance image features while suppressing background interference. We exploit image-text fusion between image features and class embeddings. The key components of the fusion modules are Text-Guided Feature Enhancement (TG-FE) and Text-Guided Query Enhancement (TG-QE), forming a text-guided encoder-decoder structure.

3.2. Image-Text Alignment

In this subsection, we focus on exploiting an effective image-text alignment approach to connect image and text features. Initially, we incorporate a text encoder to transform the class vocabulary into class embeddings. To further strengthen the connection between vision and language features, we then employ the corresponding image encoder to extract multi-scale image representations. Finally, we construct a contrastive head and introduce a image-to-text alignment loss, thereby aligning visual-semantic features in a comparable representation space.

3.2.1. Text Encoder

To incorporate class semantics into the detector, we adopt the CLIP text encoder [5, 28]. Since it contains very rich text features and is abundant for aerial image detection. The encoder accepts a class vocabulary $C \in \mathbb{R}^n$ and produces class embeddings $T = \text{TextEncoder}(C) \in \mathbb{R}^{n \times d}$, where n represents the number of class names and d denotes the dimensions of the class embeddings.

3.2.2. Image encoder

Unlike natural images, the field of aerial object detection lacks sufficient data to support training an open-vocabulary detector from scratch. To enhance visual-semantic integration and bridge the connection between visual and text features, we also incorporate the CLIP image encoder [5, 28]. Specifically, to ensure efficiency, we select the ResNet-50 version, modify it by removing the final AttnPool layer, and return the last three layers of the backbone as multi-scale feature outputs. Given an image $I \in \mathbb{R}^{H \times W \times 3}$, the extracted image features $\{F_3, F_4, F_5\} = \text{ImageEncoder}(I) \in \mathbb{R}^{H' \times W' \times C}$, where H' , W' , and C respectively denote the height, width, and channels of the feature maps.

3.2.3. Image-to-Text Alignment Loss

Contrastive Head. The contrastive head is designed to map visual-semantic features into a comparable representation space, producing similarity logit scores. Given the limited class vocabulary in aerial detection data and in order to preserve the generalization capability of the CLIP text encoder, we propose a image-to-text alignment strategy to bridge the domain gap between natural images and aerial images. Specifically, we unidirectionally align the dimensions of the visual features to the corresponding class embeddings, keeping the class embeddings unaltered. Moreover, considering the demand for efficient detection, we adopt a simple linear layer to perform the image projection.

The visual-text similarity $S(\mathbf{v}, \mathbf{t})$ is computed by:

$$S(\mathbf{v}, \mathbf{t}) = \alpha \frac{\text{proj}(\mathbf{v}) \cdot \mathbf{t}^T}{\|\text{proj}(\mathbf{v})\|_2 \cdot \|\mathbf{t}\|_2} + \beta \quad (1)$$

where \mathbf{v} is the query embedding, \mathbf{t} is the text embedding, and $\text{proj}(\cdot)$ denotes the linear layer used to align image fea-

tures with class embeddings. α and β are learnable scale and offset parameters, respectively.

This design allows us to fine-tune only a small number of learnable parameters, reducing optimization difficulty and the need for training samples, which is beneficial for overcoming the challenge of limited training samples in aerial imagery.

Detection Loss. The OVA-Det loss consists of two components: a image-to-text alignment loss and a location loss. Specifically, given an image and a set of class vocabularies, OVA-Det outputs N object predictions $\{(b_i, s_i)\}_{i=1}^N$ for each decoder, where N denotes the number of queries. The corresponding ground-truth labels for these predictions are denoted as $\{(b_k, u_k)\}_{k=1}^K$.

The image-to-text alignment loss is designed to align visual and textual features, replacing the traditional classification loss. Unlike the standard CLIP [28] pairwise image-text contrastive loss, we employ a pointwise contrastive loss that constrains the similarity score matrix between each query and the class embeddings, as obtained from the contrastive head. More specifically, considering the limited number of classes and the data constraints in aerial detection—and inspired by SigLIP [41]—we adopt sigmoid normalization instead of softmax. This conversion produces a pointwise contrastive loss and reduces dependencies among classes and batch sizes. The logits produced by the sigmoid function are then passed to the Varifocal loss [42], yielding the final image-to-text alignment loss L_{con} . We formally define L_{con} as follows:

$$L_{con}(\theta, \mathbf{u}) = \begin{cases} -\theta(u \log(\theta) + (1 - \mathbf{u}) \log(1 - \theta)), & \text{if } \mathbf{u} > 0, \\ -\alpha \theta^\gamma \log(1 - \theta), & \text{if } \mathbf{u} = 0, \end{cases} \quad (2)$$

where $\theta = \sigma(s)$, and s denotes the similarity scores predicted by the contrastive head. For a positive sample, \mathbf{u} for the ground-truth class is defined as the IoU between the predicted bounding box and its ground-truth bounding box, and 0 otherwise. For negative samples, $\mathbf{u} = 0$ for all classes.

Following previous works [43, 46], we adopt the GIoU loss L_{GIoU} and L1 loss L_{L1} for location regression. The training loss is formulated as:

$$L_{det} = \lambda L_{con} + \mu L_{GIoU} + \nu L_{L1} \quad (3)$$

where λ , μ , and ν represent the loss weights for the image-to-text alignment loss, GIOU loss, and L1 loss, respectively.

3.3. Text-Guided Strategy

By incorporating the image-text alignment approach, we have already extended detection capabilities beyond pre-defined categories. In this subsection, we further exploit text information to help the model focus on class-relevant features and enhance image-text alignment. Specifically, we propose a Text-Guided strategy, which uses textual information as guidance to reinforce aerial image features

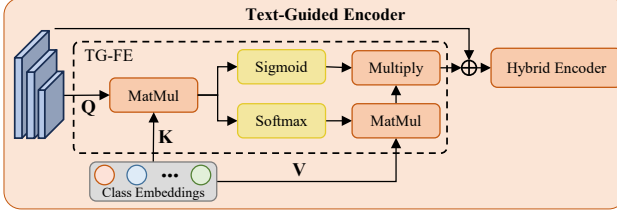


Figure 3. The Text-Guided Encoder in OVA-Det. The TG-FE enhance features extraction by incorporating relevant class semantics into image features.

and suppress background interference. We design two key components: Text-Guided Feature Enhancement (TG-FE) and Text-Guided Query Enhancement (TG-QE). The former acts on the feature extraction process and the latter works on the query, achieving simultaneous enhancement of both the encoder and decoder.

3.3.1. Text-Guided Feature Enhancement

Due to the long imaging distance in aerial imagery, the images often contain small, low-resolution targets whose visual features are not prominent, making detection relatively challenging. Additionally, the broad coverage of aerial images means that the background may contain elements that strongly interfere with the detection process. To address these two issues, we propose using text guidance to enhance visual representations and design TG-FE to operate on the encoder part.

As illustrated in Fig. 3, the core idea is based on cross attention. Specifically, given multi-scale image features $F_i \in \mathbb{R}^{H \times W \times C}$ from the image encoder and class embeddings $T \in \mathbb{R}^{N \times D}$, we employ cross-attention to fuse these modalities. To suppress the excessive injection of class embeddings into background features, we compute the maximum similarity between each image feature and the class embeddings, then apply a sigmoid function to interpret this as the probability that the image feature belongs to the foreground. We then multiply the text feature representation $T_j^{(v)}$ by this probability. The image features are updated as follows:

$$\text{Attn} = \frac{F_i^{(q)} T_j^{(k)T}}{\sqrt{d}}, \quad (4)$$

$$F'_i = F_i + \phi(\text{Attn}) \cdot T_j^{(v)} \cdot \sigma\left(\max_{j=1, \dots, n}(\text{Attn})\right), \quad (5)$$

where $F_i^{(q)}$ denotes the query projection of the i -th layer image feature in the multi-scale features, $T_j^{(k)}$ and $T_j^{(v)}$ represent the key and value projections of the text embeddings, $\phi(\cdot)$ denotes the softmax function, and $\sigma(\cdot)$ denotes the sigmoid function. Additionally, to reduce the parameter count and ensure a lightweight design, features of different scales share the same set of TG-FE parameters.

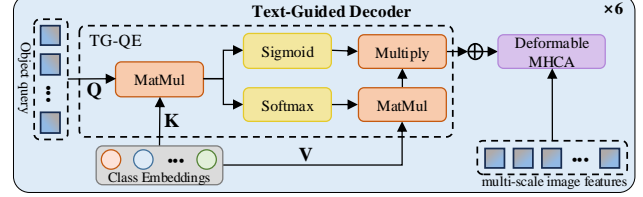


Figure 4. The Text-Guided Decoder in OVA-Det. By incorporating class information into object queries, TG-QE enables more focused retrieval of class-relevant features.

The softmax branch integrates text information into the image features, which can improve issues related to inconspicuous target visual features. Meanwhile, the sigmoid branch, guided by text information, functions like a gating mechanism, suppressing irrelevant background interference during detection. Fig. 5 visually demonstrates the impact of TG-FE on the features.

3.3.2. Text-Guided Query Enhancement

Similarly, we propose TG-QE, which operates on the decoder part. As shown in Fig. 4, TG-QE enriches object queries with class embeddings as prior knowledge so that, when these queries interact with multi-scale image features in the decoder, they can more effectively focus on class-relevant features and thus improve detection performance.

However, since the number of object queries is generally larger than the number of actual objects, most queries end up being negative samples. To avoid interference with label assignment, TG-QE adaptively suppress the injection of excessive class embeddings into these negative queries. Specifically, the object queries are updated as follows:

$$\text{Attn} = \frac{Q_i^{(q)} T_j^{(k)T}}{\sqrt{d}}, \quad (6)$$

$$Q'_i = Q_i + \phi(\text{Attn}) \cdot T_j^{(v)} \cdot \sigma\left(\max_{j=1, \dots, n}(\text{Attn})\right), \quad (7)$$

where $Q_i^{(q)}$ denotes the query projection of the i -th layer object query features in the multi-scale features, $T_j^{(k)}$ and $T_j^{(v)}$ represent the key and value projections of the text embeddings, $\phi(\cdot)$ denotes the softmax function, and $\sigma(\cdot)$ denotes the sigmoid function.

4. Experiments

In this section, we aim to demonstrate that the proposed OVA-Det has the ability to break category limitations and explicitly demonstrate the effectiveness of our proposed components. We evaluate its zero-shot detection performance on three benchmark datasets [18, 21, 35], and assess its performance in traditional object detection on the Visdrone [10] and UAVDT [9] datasets.

Method	Backbone	Source	GZSD						ZSD	
			mAP			Recall			mAP	Recall
			Base	Novel	HM	Base	Novel	HM		
RRFS[14]	ResNet-101	CVPR22	10.2	1.6	2.7	19.1	5.8	8.9	2.2	14.3
ConstrastZSD[36]	ResNet-101	TPAMI22	16.8	2.9	5.0	27.6	13.9	18.5	4.1	27.1
DescReg[40]	ResNet-101	AAAI24	17.1	5.8	8.7	28.0	12.8	17.6	8.3	43.0
Yolo-World[4]	YOLOv8-L	CVPR24	18.5	3.3	5.6	41.4	15.2	22.2	7.9	37.1
OVA-Det(Ours)	ResNet-50	-	23.8	4.7	7.9	60.7	28.3	38.6	10.9	66.1
Yolo-World*	YOLOv8-L	CVPR24	21.7	3.2	5.6	46.6	16.5	24.4	8.8	41.7
OVA-Det(Ours)*	ResNet-50	-	23.1	5.3	8.6	62.5	32.7	42.9	11.7	70.0

Table 1. Comparison with the state-of-the-art under GZSD and ZSD on xView dataset, where * denotes that the dataset split redefines the base and novel classes to avoid leakage of novel classes

Method	DIOR						DOTA					
	GZSD			ZSD			GZSD			ZSD		
	mAP		Recall		mAP		mAP		Recall		mAP	
	Base	Novel	HM	Base	Novel	HM	Base	Novel	HM	Base	Novel	HM
RRFS	41.9	2.8	5.2	60.0	19.9	29.9	9.7	19.8		47.1	2.2	4.2
ConstrastZSD	51.4	3.9	7.2	69.2	25.9	37.7	8.7	22.3		41.6	2.8	5.2
DescReg	68.7	7.9	14.2	82.0	34.3	48.4	15.2	34.6		68.7	4.7	8.8
Yolo-World-L	80.2	17.3	28.5	91.1	38.2	53.8	24.8	37.8		74.4	22.7	34.8
OVA-Det	79.6	26.1	39.3	94.4	61.5	74.4	37.2	79.8		75.5	23.7	36.1
Yolo-World-L*	78.5	3.1	5.9	91.5	18.6	30.9	6.7	20.6		71.5	1.7	3.3
OVA-Det*	79.7	7.1	13.1	94.9	52.7	67.8	14.3	75.9		72.0	2.2	4.3
										86.5	65.3	74.4
										7.8	78.8	

Table 2. Comparison with the state-of-the-art under GZSD and ZSD on DIOR and DOTA dataset, where * denotes that the dataset split redefines the base and novel classes to avoid leakage of novel classes

4.1. Datasets and Experiment Setup

Datasets. In our evaluation of zero-shot aerial object detection, we utilize three benchmark datasets: xView [18], DIOR [21], and DOTA [35]. To ensure fairness and validity in our comparative experiments, we propose two distinct protocols for splitting the datasets into base and novel classes. In the first protocol, we follow the setup from DescReg [40] to perform the class split. However, we observed that there is an overlap between the novel categories in DIOR and the base categories in DOTA, and that DOTAv1.0 lacks annotations for many small instances. To prevent leakage of novel classes and to mitigate annotation inconsistencies, in the second protocol we adopt DOTAv1.5 and adjust the category splits in DOTA accordingly. For traditional aerial object detection, OVA-Det is evaluated using the Visdrone [10] and UAVDT [9] benchmark datasets. Due to the space limitation, the results on UAVDT and the detailed base/novel category splits for each dataset are provided in the supplementary material.

Evaluation Metrics. Following [40], we utilize standard detection metrics including mean Average Precision (mAP), Recall, Harmonic Mean (HM), and Frames Per Second (FPS) for our evaluations. The mAP and Recall are com-

puted using an Intersection over Union (IoU) threshold of 0.5. The HM is computed to reflect the overall performance on base and novel classes. Additionally, we evaluate the proposed model under two evaluation settings: Zero-shot Detection (ZSD), which evaluates only novel classes, and Generalized Zero-shot Detection (GZSD), which assesses performance across both base and novel classes.

Implementation Details OVA-Det is implemented based on RT-DETR [46] with a ResNet50 backbone [13]. By incorporating an additional text encoder and contrastive loss, we form an end-to-end detection framework. All experiments were conducted on four 4090 GPUs, each with a batch size of 2. We set the number of object queries to 500 to accommodate the higher number of objects typically found in aerial images compared to natural scenes. Unless otherwise specified, the frames per second (FPS) are reported for a single 4090 GPU without the use of any additional acceleration techniques. Due to the space limitation, further details on the implementation are provided in the supplementary material.

4.2. Performance on Zero-shot Aerial Detection

As mentioned in Section 4.1, we adopt two protocols for splitting the base and novel classes. The second pro-

Method	Params	ZSD	$\text{FPS}_{bs=1}$
DescReg(Faster-RCNN)	$\geq 61\text{M}$	15.2	11
Yolo-World-L	110M	24.8	35
OVA-Det(ResNet-50)	49M	37.2	36

Table 3. Comparison of various detection methods on the DIOR dataset. Speed is tested on a 4090 GPU with no additional acceleration. Results of DescReg are taken from its original paper.

I2T Align		TG Strategy		GZSD	ZSD
C-WL	I2T Loss	TG-FE	TG-QE		
✓				2.5	3.4
✓	✓			5.6	7.0
✓	✓	✓		8.8	9.8
✓	✓		✓	10.4	12.3
✓	✓			11.5	11.3
✓	✓	✓	✓	13.1	14.3

Table 4. Ablation study of various components of our proposed method on the DIOR dataset. C-WL indicates loading CLIP encoder weights, I2T Loss represents the image-to-text alignment loss. The last two columns represent mAPs under GZSD and ZSD.

tocol is designed to avoid class leakage, and its results are marked with an asterisk (*) in the subsequent tables. For a comprehensive evaluation, we compare our approach not only with state-of-the-art aerial zero-shot detectors but also with the effective general open-vocabulary detection method YOLO-World [4].

Evaluation on xView. In Tab. 1, we compare the performance of OVA-Det with state-of-the-art methods on the **xView** dataset. In the ZSD setting, our method achieves significant improvements in both Recall and mAP, with absolute gains of 23.1% and 28.3% in Recall and 2.6% and 2.9% in mAP over the best-reported results under the first and second protocols respectively. In the GZSD setting, OVA-Det continues to demonstrate superior performance. Under the first protocol, the HM of Recall is 16.4% higher than the best-compared method. Although the HM of mAP is slightly lower than that of DescReg due to adopting a lighter backbone, our method still records the highest mAP in the base classes, and the Recall metric has nearly doubled. Under the second protocol, it surpasses YOLO-World by 3.0% in HM of mAP and 18.5% in HM of Recall.

Evaluation on DIOR and DOTA. In Tab. 2, we present the performance of OVA-Det on the **DIOR** and **DOTA** datasets. In the ZSD setting, OVA-Det demonstrates remarkable improvements in both Recall and mAP across both splits, the recall metric surpassing previous best results by 42.0%/55.3% on DIOR and 45.6%/59.3% on DOTA for the first/second split, respectively. Likewise, under the GZSD setting, OVA-Det achieves a higher HM of Recall than all compared approaches under both protocol splits,

w/ suppress		w/o suppress		GZSD	ZSD
TG-FE	TG-QE	TG-FE	TG-QE		
		✓		8.8	9.8
			✓	9.3	11.7
✓				10.4	12.3
✓			✓	11.6	12.5
✓	✓	✓	✓	13.1	14.3

Table 5. Ablation study on background interference suppression.

highlighting its strong capability for detecting novel categories. Extensive experiments across three benchmark datasets confirm that OVA-Det achieves notable performance gains in both ZSD and GZSD settings, especially in terms of Recall. These results underscore that OVA-Det offers more robust open-vocabulary detection capabilities in aerial detection.

Model Size and Latency In Tab. 3, we compare several methods on the DIOR dataset in terms of Params, ZSD mAP, and FPS. In particularly, compared to other methods, OVA-Det uses fewer parameters while achieving the highest ZSD mAP. Our model also achieves an inference speed of 36 FPS on a 4090 GPU, faster than competing methods such as DescReg and YOLO-World, and meeting the real-time detection requirements for various applications. These results highlight that OVA-Det successfully inherits the efficiency of its base architecture, making it particularly well-suited for open scenarios and aerial detection.

4.3. Ablation Study

We conduct ablation experiments on the DIOR dataset to assess the contribution of each proposed component, as shown in Tab. 4. The baseline incorporates a text encoder and a vanilla contrastive loss for image-text alignment, which enables zero-shot detection of novel classes.

Ablation on Image-to-Text Alignment. To facilitate image-text contrastive learning, we adopt CLIP-based encoders for both images and text. This improves the GZSD mAP (HM) by 3.1% and the ZSD mAP by 3.6%. Given the limited aerial detection data, we propose the image-to-text alignment loss to alleviate the challenge of image-text alignment and preserve the text encoder’s generalization capability. This further boosts the GZSD mAP (HM) and ZSD mAP by 3.2% and 2.8%, respectively. These results suggest that our proposed method effectively enhances the capability to detect novel classes in the aerial detection.

Ablation on Text-Guided Strategy. As illustrated in Tab. 4, introducing TG-FE or TG-QE individually yields notable performance improvements across both experimental settings. When both modules are employed together to form a text-guided encoder-decoder architecture, the GZSD mAP (HM) and ZSD mAP achieve 13.1% and 14.3%, respectively. These results indicate that the proposed text-

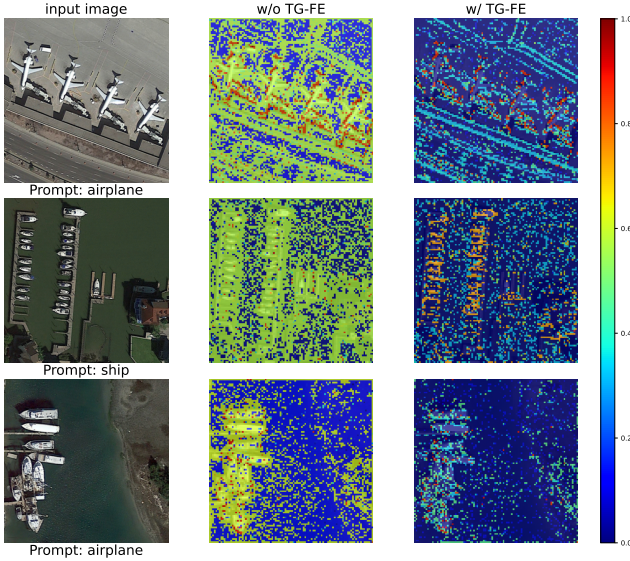


Figure 5. The impact of the TG-FE module on features. The first column displays the input images, while the subsequent two columns illustrate the correlation between the image features and the detected targets.

guided strategy enable the model to focus on class-relevant features and enhance image-text alignment.

Ablation Study on Interference Suppression. Table 5 demonstrates the effectiveness of the interference suppression branch. Experiments show that using text information as guidance to enhance features in either the encoder or decoder is effective. Compared to the baseline, this approach yields improvements of 0.5% mAP and 1.2 % mAP, respectively. Introducing the suppression branch further improves detection accuracy. For instance, for TG-FE module, introducing suppression branch further improves mAP by 1.1 percentage points.

Visual Analysis on the Impact of the proposed TG-FE. Fig.5 visualize the impact of the TG-FE module on the features. Specifically, we visualized the correlation between visual features and the text prompt before and after the introduction of the TG-FE module. The first row corresponds to cases with larger objects, while the second row corresponds to cases with smaller objects. Comparing the results in the second and third columns, it is evident that after applying the TG-FE module, the correlation between visual features and the text prompt is significantly enhanced. In particular, in the second-row example where the ship is relatively small, the initial visual features exhibited a vague correlation spread across various parts of the image. After applying TG-FE, the ship’s features became much more prominent, and the background was effectively suppressed. As shown in the third row, if the text prompt does not match the image content, the entire image is suppressed. This re-

Method	BackBone	Resolution	mAP
DMNet[19]	ResNet-50	1000×600	47.6
QueryDet[37]	ResNet-50	2400×2400	48.1
ClusDet[38]	ResNet-50	1000×600	50.6
RT-DETR[46]	ResNet-50	800×800	58.9
CZ Det[25]	ResNet-50	$800 - 1200$	58.3
UFPMP-Det[15]	ResNet-50	1333×800	62.4
GFL V1(CEASC)[8]	ResNet-18	1333×800	50.7
YOLO-World[4]	YOLOv8-L	800×800	45.0
YOLO-World[4]	YOLOv8-L	1280×1280	55.3
OVA-Det	ResNet-50	800×800	59.7
OVA-Det	ResNet-50	1280×1280	64.8

Table 6. Comparison with the state-of-the-art on the Visdrone validation set. ‘ $800 - 1200$ ’ indicates the use of multi-scale inputs.

sult, viewed from a visualization perspective, demonstrates the effectiveness of the proposed TG-FE. TG-QE is analogous to TG-FE. One operates on the encoder, and the other on the decoder; together, they work synergistically to ensure the precise detection of OVA-Det.

4.4. Performance on Traditional Aerial Detection

Although OVA-Det is designed for open vocabulary scenarios, it can also be applied to traditional aerial object detection. To this end, we conducted experiments on Visdrone to assess its performance on traditional aerial object detection, and list the results in Tab. 6. For a fair comparison with previous work, we tested using different input resolutions. At an input size of 800×800 , OVA-Det achieved an mAP of 59.7%, an improvement of 0.8% compared to RT-DETR. Increasing the resolution to 1280×1280 boosted the mAP by 2.4% beyond the previously best-reported result, achieving state-of-the-art performance. Overall, in the traditional aerial object detection field, the proposed OVA-Det still performs well; however, its performance advantage is not as significant as in the open vocabulary aerial detection field.

5. Conclusion

In this paper, we propose OVA-Det, aiming to develop an efficient open-vocabulary detector for aerial object detection. To this end, we focus on exploring image-text collaboration. Specifically, we incorporate class semantics into the detector and introduce a image-to-text alignment loss to enhance image-text alignment, thereby eliminating the predefined category constraints of traditional detectors. We further propose TG-FE and TG-QE, forming a text-guided encoder-decoder framework. This architecture makes the model focus on class-relevant features, allowing it to utilize rich textual information for improved detection performance. Moreover, by avoiding computationally intensive modules, OVA-Det inherits the efficiency of its base-

line, meets the real time demand of aerial detection, and is therefore more suitable for open scenarios. In future work, we will further explore text guidance, extending word-level cues to phrases and even sentences to provide more detailed guidance information, thereby enhancing open detection capabilities while broadening the model’s applicability.

References

[1] Zhaowei Cai and Nuno Vasconcelos. Cascade r-cnn: Delving into high quality object detection. In *Proceedings of the IEEE conference on computer vision and pattern recognition*, pages 6154–6162, 2018. [2](#)

[2] Nicolas Carion, Francisco Massa, Gabriel Synnaeve, Nicolas Usunier, Alexander Kirillov, and Sergey Zagoruyko. End-to-end object detection with transformers. In *European conference on computer vision*, pages 213–229, 2020. [2](#)

[3] Fangyi Chen, Han Zhang, Zhantao Yang, Hao Chen, Kai Hu, and Marios Savvides. Rtnet: Generating region-text pairs for open-vocabulary object detection. *arXiv preprint arXiv:2405.19854*, 2024. [2](#)

[4] Tianheng Cheng, Lin Song, Yixiao Ge, Wenyu Liu, Xinggang Wang, and Ying Shan. Yolo-world: Real-time open-vocabulary object detection. In *Proceedings of the IEEE/CVF Conference on Computer Vision and Pattern Recognition*, pages 16901–16911, 2024. [1, 2, 6, 7, 8, 14](#)

[5] Mehdi Cherti, Romain Beaumont, Ross Wightman, Mitchell Wortsman, Gabriel Ilharco, Cade Gordon, Christoph Schuhmann, Ludwig Schmidt, and Jenia Jitsev. Reproducible scaling laws for contrastive language-image learning. In *Proceedings of the IEEE/CVF Conference on Computer Vision and Pattern Recognition*, pages 2818–2829, 2023. [4](#)

[6] Sutao Deng, Shuai Li, Ke Xie, Wenfeng Song, Xiao Liao, Aimin Hao, and Hong Qin. A global-local self-adaptive network for drone-view object detection. *IEEE Transactions on Image Processing*, 30:1556–1569, 2020. [14](#)

[7] Jian Ding, Nan Xue, Gui-Song Xia, Xiang Bai, Wen Yang, Michael Ying Yang, Serge Belongie, Jiebo Luo, Mihai Datcu, Marcello Pelillo, et al. Object detection in aerial images: A large-scale benchmark and challenges. *IEEE transactions on pattern analysis and machine intelligence*, 44(11):7778–7796, 2021. [1](#)

[8] Bowei Du, Yecheng Huang, Jiaxin Chen, and Di Huang. Adaptive sparse convolutional networks with global context enhancement for faster object detection on drone images. In *Proceedings of the IEEE/CVF conference on computer vision and pattern recognition*, pages 13435–13444, 2023. [3, 8, 14](#)

[9] Dawei Du, Yuankai Qi, Hongyang Yu, Yifan Yang, Kaiwen Duan, Guorong Li, Weigang Zhang, Qingming Huang, and Qi Tian. The unmanned aerial vehicle benchmark: Object detection and tracking. In *Proceedings of the European conference on computer vision (ECCV)*, pages 370–386, 2018. [5, 6, 14](#)

[10] Dawei Du, Pengfei Zhu, Longyin Wen, Xiao Bian, Haibin Lin, Qinghua Hu, Tao Peng, Jiayu Zheng, Xinyao Wang, Yue Zhang, et al. Visdrone-det2019: The vision meets drone object detection in image challenge results. In *Proceedings of the IEEE/CVF international conference on computer vision workshops*, pages 0–0, 2019. [5, 6](#)

[11] Xiuye Gu, Tsung-Yi Lin, Weicheng Kuo, and Yin Cui. Open-vocabulary object detection via vision and language knowledge distillation. *arXiv preprint arXiv:2104.13921*, 2021. [1, 2](#)

[12] Kai Han, Yandong Li, Sagar Vaze, Jie Li, and Xuhui Jia. What’s in a name? beyond class indices for image recognition. *arXiv preprint arXiv:2304.02364*, 2023. [1, 2](#)

[13] Kaiming He, Xiangyu Zhang, Shaoqing Ren, and Jian Sun. Deep residual learning for image recognition. In *Proceedings of the IEEE conference on computer vision and pattern recognition*, pages 770–778, 2016. [6, 13](#)

[14] Peiliang Huang, Junwei Han, De Cheng, and Dingwen Zhang. Robust region feature synthesizer for zero-shot object detection. In *Proceedings of the IEEE/CVF conference on computer vision and pattern recognition*, pages 7622–7631, 2022. [6](#)

[15] Yecheng Huang, Jiaxin Chen, and Di Huang. Ufpmp-det: Toward accurate and efficient object detection on drone imagery. In *Proceedings of the AAAI conference on artificial intelligence*, pages 1026–1033, 2022. [1, 3, 8, 14](#)

[16] Drew A Hudson and Christopher D Manning. Gqa: A new dataset for real-world visual reasoning and compositional question answering. In *Proceedings of the IEEE/CVF conference on computer vision and pattern recognition*, pages 6700–6709, 2019. [14](#)

[17] Chao Jia, Yinfai Yang, Ye Xia, Yi-Ting Chen, Zarana Parekh, Hieu Pham, Quoc Le, Yun-Hsuan Sung, Zhen Li, and Tom Duerig. Scaling up visual and vision-language representation learning with noisy text supervision. In *International conference on machine learning*, pages 4904–4916. PMLR, 2021. [2](#)

[18] Darius Lam, Richard Kuzma, Kevin McGee, Samuel Doolley, Michael Laielli, Matthew Klaric, Yaroslav Bulatov, and Brendan McCord. Xview: Objects in context in overhead imagery. *arXiv preprint arXiv:1802.07856*, 2018. [5, 6, 12](#)

[19] Changlin Li, Taojiaannan Yang, Sijie Zhu, Chen Chen, and Shanyue Guan. Density map guided object detection in aerial images. In *proceedings of the IEEE/CVF conference on computer vision and pattern recognition workshops*, pages 190–191, 2020. [1, 3, 8, 14](#)

[20] Jiameng Li, Jiacheng Zhang, Jichang Li, Ge Li, Si Liu, Liang Lin, and Guanbin Li. Learning background prompts to discover implicit knowledge for open vocabulary object detection. In *Proceedings of the IEEE/CVF Conference on Computer Vision and Pattern Recognition*, pages 16678–16687, 2024. [2](#)

[21] Ke Li, Gang Wan, Gong Cheng, Liqiu Meng, and Junwei Han. Object detection in optical remote sensing images: A survey and a new benchmark. *ISPRS journal of photogrammetry and remote sensing*, 159:296–307, 2020. [1, 5, 6, 12](#)

[22] Liunian Harold Li, Pengchuan Zhang, Haotian Zhang, Jianwei Yang, Chunyuan Li, Yiwu Zhong, Lijuan Wang, Lu Yuan, Lei Zhang, Jenq-Neng Hwang, et al. Grounded language-image pre-training. In *Proceedings of the IEEE/CVF Conference on Computer Vision and Pattern Recognition*, pages 10965–10975, 2022. [1, 2, 13](#)

[23] Yan Li, Weiwei Guo, Dunyun He, Jiaqi Zhou, Yuze Gao, and Wenxian Yu. Castdet: Toward open vocabulary aerial object detection with clip-activated student-teacher learning. *arXiv preprint arXiv:2311.11646*, 2023. 2, 3

[24] Shilong Liu, Zhaoyang Zeng, Tianhe Ren, Feng Li, Hao Zhang, Jie Yang, Qing Jiang, Chunyuan Li, Jianwei Yang, Hang Su, et al. Grounding dino: Marrying dino with grounded pre-training for open-set object detection. In *European Conference on Computer Vision*, pages 38–55. Springer, 2024. 1, 2

[25] Akhil Meethal, Eric Granger, and Marco Pedersoli. Cascaded zoom-in detector for high resolution aerial images. In *Proceedings of the IEEE/CVF Conference on Computer Vision and Pattern Recognition*, pages 2046–2055, 2023. 1, 8

[26] Jiancheng Pan, Yanxing Liu, Yuqian Fu, Muyuan Ma, Jiaohao Li, Danda Pani Paudel, Luc Van Gool, and Xiaomeng Huang. Locate anything on earth: Advancing open-vocabulary object detection for remote sensing community. *arXiv preprint arXiv:2408.09110*, 2024. 2, 3

[27] Bryan A Plummer, Liwei Wang, Chris M Cervantes, Juan C Caicedo, Julia Hockenmaier, and Svetlana Lazebnik. Flickr30k entities: Collecting region-to-phrase correspondences for richer image-to-sentence models. In *Proceedings of the IEEE international conference on computer vision*, pages 2641–2649, 2015. 14

[28] Alec Radford, Jong Wook Kim, Chris Hallacy, Aditya Ramesh, Gabriel Goh, Sandhini Agarwal, Girish Sastry, Amanda Askell, Pamela Mishkin, Jack Clark, et al. Learning transferable visual models from natural language supervision. In *International conference on machine learning*, pages 8748–8763. PMLR, 2021. 1, 2, 4

[29] Shaoqing Ren, Kaiming He, Ross Girshick, and Jian Sun. Faster r-cnn: Towards real-time object detection with region proposal networks. *Advances in neural information processing systems*, 28, 2015. 2

[30] Edmund J Sadgrove, Greg Falzon, David Miron, and David W Lamb. Real-time object detection in agricultural/remote environments using the multiple-expert colour feature extreme learning machine (mec-elm). *Computers in Industry*, 98:183–191, 2018. 1

[31] Shuai Shao, Zeming Li, Tianyuan Zhang, Chao Peng, Gang Yu, Xiangyu Zhang, Jing Li, and Jian Sun. Objects365: A large-scale, high-quality dataset for object detection. In *Proceedings of the IEEE/CVF international conference on computer vision*, pages 8430–8439, 2019. 14

[32] Piyush Sharma, Nan Ding, Sebastian Goodman, and Radu Soricut. Conceptual captions: A cleaned, hypernymed, image alt-text dataset for automatic image captioning. In *Proceedings of the 56th Annual Meeting of the Association for Computational Linguistics (Volume 1: Long Papers)*, pages 2556–2565, 2018. 14

[33] Zhiwei Wei, Chenzhen Duan, Xinghao Song, Ye Tian, and Hongpeng Wang. Amrnet: Chips augmentation in aerial images object detection. *arXiv preprint arXiv:2009.07168*, 2020. 14

[34] Size Wu, Wenwei Zhang, Sheng Jin, Wentao Liu, and Chen Change Loy. Aligning bag of regions for open-vocabulary object detection. In *Proceedings of the IEEE/CVF conference on computer vision and pattern recognition*, pages 15254–15264, 2023. 2

[35] Gui-Song Xia, Xiang Bai, Jian Ding, Zhen Zhu, Serge Beßongie, Jiebo Luo, Mihai Datcu, Marcello Pelillo, and Liangpei Zhang. Dota: A large-scale dataset for object detection in aerial images. In *Proceedings of the IEEE conference on computer vision and pattern recognition*, pages 3974–3983, 2018. 5, 6, 12

[36] Caixia Yan, Xiaojun Chang, Minnan Luo, Huan Liu, Xiaoqin Zhang, and Qinghua Zheng. Semantics-guided contrastive network for zero-shot object detection. *IEEE transactions on pattern analysis and machine intelligence*, 46(3):1530–1544, 2022. 6

[37] Chenhongyi Yang, Zehao Huang, and Naiyan Wang. Query-det: Cascaded sparse query for accelerating high-resolution small object detection. In *Proceedings of the IEEE/CVF Conference on computer vision and pattern recognition*, pages 13668–13677, 2022. 8

[38] Fan Yang, Heng Fan, Peng Chu, Erik Blasch, and Haibin Ling. Clustered object detection in aerial images. In *Proceedings of the IEEE/CVF international conference on computer vision*, pages 8311–8320, 2019. 1, 3, 8, 14

[39] Lewei Yao, Jianhua Han, Xiaodan Liang, Dan Xu, Wei Zhang, Zhenguo Li, and Hang Xu. Detclipv2: Scalable open-vocabulary object detection pre-training via word-region alignment. In *Proceedings of the IEEE/CVF Conference on Computer Vision and Pattern Recognition*, pages 23497–23506, 2023. 2

[40] Zhengqing Zang, Chenyu Lin, Chenwei Tang, Tao Wang, and Jiancheng Lv. Zero-shot aerial object detection with visual description regularization. In *Proceedings of the AAAI Conference on Artificial Intelligence*, pages 6926–6934, 2024. 2, 3, 6, 12, 14

[41] Xiaohua Zhai, Basil Mustafa, Alexander Kolesnikov, and Lucas Beyer. Sigmoid loss for language image pre-training. In *Proceedings of the IEEE/CVF International Conference on Computer Vision*, pages 11975–11986, 2023. 4

[42] Haoyang Zhang, Ying Wang, Feras Dayoub, and Niko Sunderhauf. Varifocalnet: An iou-aware dense object detector. In *Proceedings of the IEEE/CVF conference on computer vision and pattern recognition*, pages 8514–8523, 2021. 4

[43] Hao Zhang, Feng Li, Shilong Liu, Lei Zhang, Hang Su, Jun Zhu, Lionel M Ni, and Heung-Yeung Shum. Dino: Detr with improved denoising anchor boxes for end-to-end object detection. *arXiv preprint arXiv:2203.03605*, 2022. 2, 4

[44] Haotian Zhang, Pengchuan Zhang, Xiaowei Hu, Yen-Chun Chen, Liunian Li, Xiyang Dai, Lijuan Wang, Lu Yuan, Jenq-Neng Hwang, and Jianfeng Gao. Glipv2: Unifying localization and vision-language understanding. *Advances in Neural Information Processing Systems*, 35:36067–36080, 2022. 2

[45] Shiyu Zhao, Zhixing Zhang, Samuel Schulter, Long Zhao, BG Vijay Kumar, Anastasis Stathopoulos, Manmohan Chandraker, and Dimitris N Metaxas. Exploiting unlabeled data with vision and language models for object detection. In *European conference on computer vision*, pages 159–175, 2022. 1, 2

- [46] Yian Zhao, Wenyu Lv, Shangliang Xu, Jinman Wei, Guanzhong Wang, Qingqing Dang, Yi Liu, and Jie Chen. Detrs beat yolos on real-time object detection. In *Proceedings of the IEEE/CVF Conference on Computer Vision and Pattern Recognition*, pages 16965–16974, 2024. [2](#), [4](#), [6](#), [8](#), [13](#), [14](#)
- [47] Yiwu Zhong, Jianwei Yang, Pengchuan Zhang, Chunyuan Li, Noel Codella, Liunian Harold Li, Luowei Zhou, Xiyang Dai, Lu Yuan, Yin Li, et al. Regionclip: Region-based language-image pretraining. In *Proceedings of the IEEE/CVF conference on computer vision and pattern recognition*, pages 16793–16803, 2022. [2](#)

OVA-Det: Open Vocabulary Aerial Object Detection with Image-Text Collaboration

Supplementary Material

6. Dataset Details

6.1. Zero-shot Detection Dataset Details

To ensure a fair experimental comparison, we followed the state-of-the-art DescReg [40] for open aerial object detection to organize our experiments. We evaluate OVA-Det zero-shot detection performance on three benchmark datasets. The dataset details as follows:

- **xView** [18] comprises high resolution satellite images captured by the WorldView-3 satellite at a 0.3m ground sample distance. The resolutions in xView range from about 2500×2500 to 5000×3500 pixels. The dataset includes 846 annotated images with 60 classes. We selected 665 images for training and 181 for evaluation.
- **DIOR** [21] is a large-scale benchmark dataset for aerial object detection, with the resolution of 800×800 . It consists of 5862 training images, 5863 validation images, and 11,725 test images, with 20 annotated classes. We conducted training on the training set and evaluation on the validation set.
- **DOTA** [35] consists of satellite images with resolutions ranging from 800×800 to 4000×4000 . In this work, we employ both DOTAv1.0 and DOTAv1.5, which share the same set of 1411 training images and 458 validation images, but differ in that DOTAv1.5 includes additional annotations for very small objects.

6.1.1. Dataset Crop Details

For the xView and DOTA datasets, due to their high image resolutions, we simplified the datasets by cropping images during pre-processing. Following prior work [40], we cropped the images in these datasets to a size of 800×800 . Ultimately, we obtained 12,825 training images and 3,550 test images for xView, and 18,430 training and 6,259 test images for DOTA, respectively.

6.1.2. Dataset Base/Novel Split Details

For the xView and DIOR datasets, we followed the setup from prior work [40] to split base and novel classes. The resulting category splits are 48/12 and 16/4 for xView and DIOR, respectively. The class splits are:

- **xView dataset:**
 - Base: 'fixed wing aircraft', 'small aircraft', 'passenger plane or cargo plane', 'passenger vehicle', 'small car', 'utility truck', 'truck', 'cargo truck', 'truck tractor', 'trailer', 'truck tractor with flatbed trailer', 'truck tractor with liquid tank', 'crane truck', 'railway vehicle', 'passenger car', 'cargo car

or container car', 'flat car', 'tank car', 'locomotive', 'sailboat', 'tugboat', 'fishing vessel', 'ferry', 'yacht', 'container ship', 'oil tanker', 'engineering vehicle', 'tower crane', 'container crane', 'straddle carrier', 'dump truck', 'haul truck', 'front loader or bulldozer', 'cement mixer', 'ground grader', 'hut or tent', 'shed', 'building', 'aircraft hangar', 'damaged building', 'facility', 'construction site', 'vehicle lot', 'helipad', 'storage tank', 'shipping container', 'pylon', 'tower'.

- Novel: 'helicopter', 'bus', 'pickup truck', 'truck tractor with box trailer', 'maritime vessel', 'motorboat', 'barge', 'reach stacker', 'mobile crane', 'scraper or tractor', 'excavator', 'shipping container lot'.

• **DIOR dataset:**

- Base: 'airplane', 'baseball field', 'bridge', 'chimney', 'dam', 'Expressway Service area', 'Expressway toll station', 'goldfield', 'harbor', 'overpass', 'ship', 'stadium', 'storage tank', 'tennis court', 'train station', 'vehicle'.
- Novel: 'airport', 'basketball court', 'ground track field', 'windmill'.

For the DOTA dataset, we observed overlaps between the novel categories in DIOR and the base categories in prior DOTA splits. In addition, DOTAv1.0 lacks annotations for many small instances. Therefore, we adopt DOTAv1.5 and adjust the category splits to prevent novel class leakage and reduce annotation inconsistencies. As a result, the revised splits yield 12 base classes and 4 novel classes for the DOTA dataset.

• **DOTA dataset:**

- Base: 'plane', 'ship', 'storage tank', 'baseball diamond', 'basketball court', 'ground track field', 'harbor', 'bridge', 'large vehicle', 'small vehicle', 'roundabout'.
- Novel: 'tennis court', 'helicopter', 'soccer ball field', 'swimming pool'.

• **DOTA dataset resplit:**

- Base: 'plane', 'ship', 'storage tank', 'baseball diamond', 'tennis court', 'soccer ball field', 'harbor', 'bridge', 'large vehicle', 'small vehicle', 'roundabout', 'container crane'.
- Novel: 'basketball court', 'helicopter', 'ground track field', 'swimming pool'.

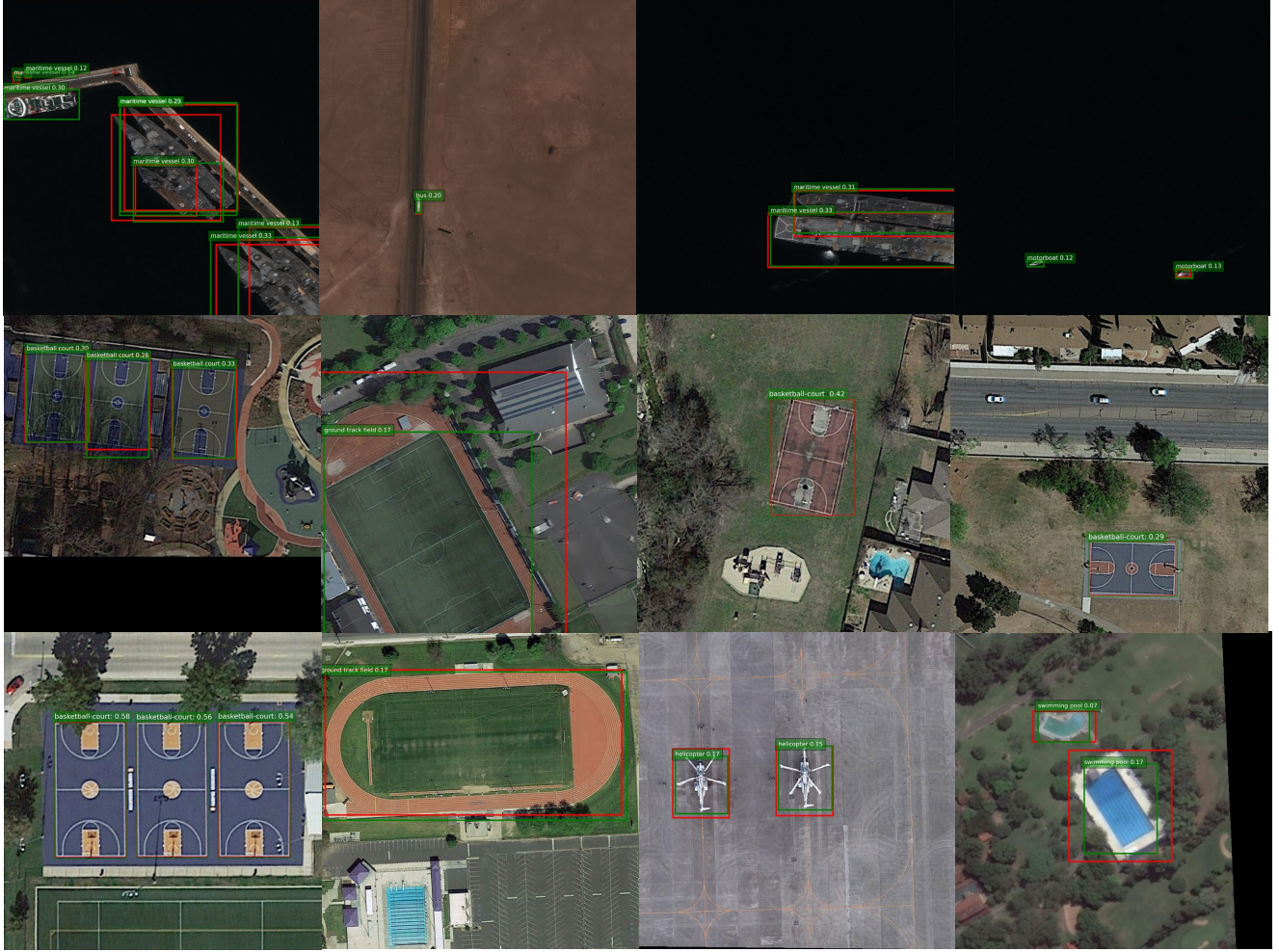


Figure 6. Qualitative results for zero-shot detection on the xView, DIOR, and DOTA datasets, focusing on novel classes. The green rectangles represent predicted bounding boxes, while red rectangles denote ground truth bounding boxes.

7. Qualitative Results

As shown in Fig 6, we present qualitative results of OVA-Det on the xView, DIOR, and DOTA datasets. The images in the first, second, and third rows correspond to xView, DIOR, and DOTA, respectively. These results demonstrate that our proposed method breaks the category limitations of traditional detectors and can accurately detect novel classes. As can be seen, even for targets with inconspicuous visual features, such as the bus and motorboat in the first row, our proposed OVA-Det can still detect them.

8. Implementation Details

8.1. Training Details

The OVA-Det implementation is based on RT-DETR [46] with a ResNet50 [13] backbone, using the default hyperparameters provided by RT-DETR. In the query selection

module, we replace classification scores with image-text similarity scores to select the top 500 encoder features, which are then used to initialize the object queries for the decoder. We also use these similarity scores instead of classification scores for label assignment. We employ a one-stage training scheme, excluding novel classes from the training sets of all three datasets for training. The model is evaluated on both GZSD and ZSD tasks using the test sets of these three datasets.

Following the approach in [22], we adopt a random class sampling procedure during training. Specifically, we shuffle the order of input text each time, preventing the model from relying on fixed positions of class embeddings. We first sample the positive classes that appear in the images, and then randomly sample the remaining negative classes to reach the required number of training classes. If there are insufficient negative classes, we use an empty token as a placeholder and mask the corresponding class embeddings

in subsequent operations.

8.2. Details of the compared method

Due to the unavailability of the code from prior work [40], we directly use the results reported in their publication for experiments under their dataset split. YOLO-World [4] is the most effective OVD method for natural images. We compare our model against it to demonstrate the OVA-Det’s suitability for aerial OVD tasks. Specifically, we follow the training procedures detailed in their published paper and available code, conducting experiments under settings similar to ours.

To highlight the advantages of our approach, we use the versions of each method that have been pretrained on the largest amount of data (for example, a YOLO-World model pretrained on Objects365V1 [31], GQA [16], Flickr [27], and CC3M [32]). We then fine-tune these models on the three aerial image datasets.

9. More Experimental Results

9.1. Comparison with RT-DETR

As described in the main text, our method follows the RT-DETR framework. Therefore, we compare OVA-Det and RT-DETR in terms of model size, detection accuracy, and inference speed. Since RT-DETR cannot be applied to open vocabulary scenarios, we conducted closed-world comparison experiments on Visdrone. The corresponding results are listed in Table 7.

Based on the experimental results, our method can also improve detection accuracy in closed scenarios. To accommodate open scenarios, additional parameters and computational overhead were introduced. Image-to-text alignment loss introduced about 2M parameters, TG-FE and TG-QE introduced about 6M parameters. However, since the additional modules are all linear structures, the hardware inference speed is relatively fast. Therefore, the model’s latency increase is minimal, with an FPS reduction of about 5 frames. Ultimately, it maintains an inference speed of 36 FPS, which is sufficient to meet the real-time inference requirements of typical videos (25–30 FPS).

9.2. Performance on UAVDT dataset

UAVDT [9] is also a benchmark for evaluation in aerial object detection. The dataset comprises 23,258 training images and 15,069 testing images with a resolution of 1024×540 , covering 3 classes.

Besides Visdrone, to further demonstrate the performance of OVA-Det on traditional aerial detection tasks, we evaluate our method on the UAVDT dataset. As shown in Table 8, OVA-Det achieves the highest mAP performance, surpassing the best-compared method by 0.5% in mAP. In summary, our proposed OVA-Det not only adapts to open-

Method	Params	mAP	FPS _{bs=1}
RT-DETR(ResNet-50)	41M	58.9	41
OVA-Det(ResNet-50)	49M	59.7	36

Table 7. Comparison of OVA-Det and RT-DETR on the Visdrone Dataset.

Method	BackBone	Resolution	mAP
DMNet[19]	ResNet-50	1000×600	24.6
ClusDet[38]	ResNet-50	1000×600	26.5
GLSAN[6]	ResNet-50	1000×600	28.1
ARMNet[33]	ResNet-50	1500×800	30.4
RT-DETR[46]	ResNet-50	800×800	39.5
UFPMMP-Det[15]	ResNet-50	1000×600	38.7
GFL V1(CEASC)[8]	ResNet-18	1024×540	30.9
YOLO-World[4]	YOLOv8-L	800×800	35.8
OVA-Det	ResNet-50	800×800	41.0

Table 8. Comparison with the state-of-the-art on the UAVDT dataset.

vocabulary aerial object detection scenarios but also retains excellent performance in closed settings.